



## Original article

## Hapln1 promotes dedifferentiation and proliferation of iPSC-derived cardiomyocytes by promoting versican-based GDF11 trapping

Ding-Jun Hao <sup>a,1</sup>, Yue Qin <sup>b,1</sup>, Shi-Jie Zhou <sup>d</sup>, Bu-Huai Dong <sup>b</sup>, Jun-Song Yang <sup>a</sup>, Peng Zou <sup>a</sup>, Li-Ping Wang <sup>c</sup>, Yuan-Ting Zhao <sup>a,\*</sup><sup>a</sup> Department of Spine Surgery, Honghui Hospital, Xi'an Jiaotong University, Xi'an, 710054, China<sup>b</sup> Department of Anesthesiology, Honghui Hospital, Xi'an Jiaotong University, Xi'an, 710054, China<sup>c</sup> Department of Cardiovascular Medicine, Honghui Hospital, Xi'an Jiaotong University, Xi'an, 710054, China<sup>d</sup> State Key Laboratory of Biotherapy/Collaborative Innovation Center for Biotherapy, West China Hospital, Sichuan University, Chengdu, 610041, China

## ARTICLE INFO

## Article history:

Received 7 April 2023

Received in revised form

8 July 2023

Accepted 18 September 2023

Available online 22 September 2023

## Keywords:

Hapln1

Versican

GDF11

iPSC-CMs

Cardiomyocyte proliferation

## ABSTRACT

Hyaluronan and proteoglycan link protein 1 (Hapln1) supports active cardiomyogenesis in zebrafish hearts, but its regulation in mammal cardiomyocytes is unclear. This study aimed to explore the potential regulation of Hapln1 in the dedifferentiation and proliferation of cardiomyocytes and its therapeutic value in myocardial infarction with human induced pluripotent stem cell (hiPSC)-derived cardiomyocytes (CMs) and an adult mouse model of myocardial infarction. HiPSC-CMs and adult mice with myocardial infarction were used as *in vitro* and *in vivo* models, respectively. Previous single-cell RNA sequencing data were retrieved for bioinformatic exploration. The results showed that recombinant human Hapln1 (rhHapln1) promotes the proliferation of hiPSC-CMs in a dose-dependent manner. As a physical binding protein of Hapln1, versican interacted with Nodal growth differentiation factor (NODAL) and growth differentiation factor 11 (GDF11). GDF11, but not NODAL, was expressed by hiPSC-CMs. GDF11 expression was unaffected by rhHapln1 treatment. However, this molecule was required for rhHapln1-mediated activation of the transforming growth factor (TGF)- $\beta$ /Drosophila mothers against decapentaplegic protein (SMAD)2/3 signaling in hiPSC-CMs, which stimulates cell dedifferentiation and proliferation. Recombinant mouse Hapln1 (rmHapln1) could induce cardiac regeneration in the adult mouse model of myocardial infarction. In addition, rmHapln1 induced hiPSC-CM proliferation. In conclusion, Hapln1 can stimulate the dedifferentiation and proliferation of iPSC-derived cardiomyocytes by promoting versican-based GDF11 trapping and subsequent activation of the TGF- $\beta$ /SMAD2/3 signaling pathway. Hapln1 might be an effective hiPSC-CM dedifferentiation and proliferation agent and a potential reagent for repairing damaged hearts.

© 2023 The Authors. Published by Elsevier B.V. on behalf of Xi'an Jiaotong University. This is an open access article under the CC BY-NC-ND license (<http://creativecommons.org/licenses/by-nc-nd/4.0/>).

## 1. Introduction

Human cardiomyocytes are terminally differentiated, with a limited proliferative capacity [1]. Therefore, cardiac injury and heart failure cannot be adequately repaired by the proliferation of endogenous cardiomyocytes [1,2]. Induced pluripotent stem cell (iPSC)-derived cardiomyocytes (CMs) can recapitulate patient-specific phenotypes, making them invaluable for disease modeling and drug testing [3,4]. In addition, these cells provide an

unprecedented opportunity for potential cardiovascular regenerative therapy via cellular transplantation [4].

One advantage of using iPSC-CMs for cardiac therapy is their potential ability to proliferate and generate new heart muscle cells. This ability could be particularly useful in cases where there is extensive damage to the heart tissue, and iPSC-CMs might be used to replace the damaged tissue and restore cardiac function [3,4]. However, the immature state is one of the major hurdles in the clinical translation of iPSC-CMs. Some strategies have been used to promote structural, electrophysiological, and metabolic maturation, such as *in vivo* transplantation and 3D tissue engineering [5,6]. These strategies stimulate maturation by mimicking normal embryonic heart development and postnatal hypertrophy [6]. However, proliferation and maturation are two sides of the same coin

Peer review under responsibility of Xi'an Jiaotong University.

\* Corresponding author.

E-mail address: [doczhaoyuanting@126.com](mailto:doczhaoyuanting@126.com) (Y.-T. Zhao).<sup>1</sup> Both authors contributed equally to this work.

for cardiomyocytes [6]. The maturation of iPSC-CMs is associated with lost proliferative capability [5,6]. A clear understanding of the underlying mechanisms would help manipulate the proliferation/maturation process and facilitate the clinical translation of this technology.

The regulatory effects of extracellular matrix (ECM) and associated signaling on the proliferation of embryonic and fetal mammalian cardiomyocytes have been gradually revealed. The proteoglycans and glycoproteins might play critical roles in the heart muscle proliferation. Agrin, a proteoglycan and a component of neonatal ECM, promotes the division of cardiomyocytes and stimulates cardiac regeneration in adult mice after myocardial infarction [7]. Hyaluronan and proteoglycan link protein 1 (Hapln1) was initially identified as a cartilage link protein from the proteoglycan component of bovine articular cartilage [8]. This molecule positively regulates the stability, binding activity, and organization of two critical ECM macromolecules, hyaluronan (HA) and proteoglycan [9].

Previous studies have revealed the role of Hapln1 in heart development [10,11]. *HAPLN1* knockdown mice presented a series of cardiac malformations, such as atrioventricular junction septal and myocardial defects, with a drastically decreased concentration of versican, an ECM component essential for cardiac development [10]. The asymmetric spatial expression of Hapln1 promotes correct heart morphogenesis in a zebrafish model [11]. Zebrafish heart has exceptionally high regenerative capacity since the adult cardiomyocytes can dedifferentiate and proliferate after major injuries [12]. One recent study has linked Hapln1 expression with heart regeneration in zebrafish [13]. A subset of postembryonic epicardial cells highly expressed hapln1 paralogs, which directly support active cardiomyogenesis in the surrounding regions in the contexts of heart morphogenesis and injury-induced regeneration. This mechanism might be related to the positive effects of Hapln1 on HA deposition [13].

Mammalian heart injury typically leads to scarring, with minimal regeneration of heart muscle. Whether Hapln1 stimulates cardiomyocyte differentiation and proliferation of mammal cardiomyocytes is not clear. Using human iPSC-CMs (hiPSC-CMs) and myocardial infarction in adult mice, we aimed to explore the potential regulation of Hapln1 in the dedifferentiation and proliferation of cardiomyocytes and its therapeutic value in myocardial infarction.

## 2. Materials and methods

### 2.1. Cell culture and treatment

LHpb-YaabC3 hiPSC (HNF-P30-P11) and HN4 human embryonic stem cell (hESC) lines (HES-P20-P9) were purchased from Osinglay Bio-Pharmaceutical (Guangzhou, China). Lentiviral plasmids for *VCAN* knockdown were generated using the pLKO.1-puro plasmid, with the following validated short hairpin RNA (shRNA) sequences: shVCAN (human), 5'-GTGAATTTCTCCGCATCAAAT-3'; shHAPLN1 (mouse), 5'-CCAGATCAAGACAGAGTTATT-3'; and shRNA scrambled control (shNC), 5'-CCTAAGGTTAAGTCGCCCTCG-3'. Lentiviruses were produced by cotransfecting the recombinant plasmids, the packaging plasmid psPAX2, and the envelope plasmid, pMD2.G, into the packaging 293T cell line. Cell supernatant was collected 48 and 72 h after transfection, filtered through 0.45  $\mu\text{m}$  filters, centrifuged, and stored at  $-80^\circ\text{C}$  before use.

### 2.2. Preparation of cardiomyocytes differentiated from hiPSCs

Cardiomyocyte differentiation was conducted in a growth factor and serum-free system following the Gsk3 inhibitor and Wnt

inhibitor (GiwI) protocol [14], in which the canonical Wnt signaling pathway was manipulated using a Gi and Wi.

For hypoxia treatment, iPSC-CMs after indicating culture periods were subjected to hypoxic culture (1% O<sub>2</sub>, 5% CO<sub>2</sub>, 94% N<sub>2</sub>) for 24 h and reoxygenation for 6 h. Then, the cells were subjected to cell counting kit (CCK)-8 assays for cell viability and lactate dehydrogenase (LDH) cytotoxicity assays. Recombinant human Hapln1 (rhHapln1) protein was obtained from Sino Biological (10323-H08H; Beijing, China). Recombinant mouse HAPLN1 (rmHAPLN1), human growth differentiation factor 11 (GDF11), and human Nodal growth differentiation factor (NODAL) protein were obtained from CUSABIO (CSB-EP010130MO, CSB-EP009344HU, and CSB-EP850428HU; Wuhan, China).

A-83-01, a potent inhibitor of the transforming growth factor (TGF)- $\beta$  type I receptor ALK5, ALK4, and ALK7 kinase and GDF11 was purchased from MedChemExpress (Monmouth Junction, NJ, USA). GDF11 neutralizing antibody was purchased from Creative BioLabs (CAT#: NEUT-859CQ; Shirley, NY, USA).

### 2.3. Primary cell culture

Protocols for animal experiments were approved by the Ethics Committee of the Honghui Hospital, China, and the Chengdu Jinruijie Biotechnology Service Center, China (Approval No.: 202206018). The Institutional Guidelines for the Care and Use of Laboratory Animals were strictly adhered to for all animal housing and experiments. Standard specific pathogen free (SPE) conditions were maintained for the mice, with temperatures of about 18–23  $^\circ\text{C}$  and 40%–60% humidity. Anesthesia was induced via isoflurane inhalation in postnatal day 1 (P1), P7, P14, and P35 C57BL/6 mice. The Pierce Primary Cardiomyocyte Isolation Kit (#88281; Thermo Fisher Scientific Inc., Carlsbad, CA, USA) was used to isolate primary cardiomyocytes and primary cardiac fibroblasts according to the manufacturer's instructions. All isolated fibroblasts were cultured in fibroblast medium (10% fetal bovine serum in Dulbecco's modified Eagle medium) for three passages to increase their purity before use.

### 2.4. Immunofluorescence staining

Immunofluorescence staining was performed following the methods introduced previously [15]. Briefly, hiPSCs and induced hiPSC-CMs were seeded in an ibidi  $\mu$ -Slide 8 Well coated with Matrigel (80806; ibidi, Gräfelfing, Germany). For *in vitro* EdU incorporation, EdU (10  $\mu\text{M}$ ) was added 24 h before fluorescence detection. Then, cells were fixed with 4% (*m/V*) paraformaldehyde, permeabilized, blocked and then incubated with the following primary antibodies and dilutions at 4  $^\circ\text{C}$  overnight: anti-NK2 Homeobox 5 (NKX2.5) (1:500, #8792; Cell Signaling Technology, Danvers, MA, USA), anti- $\alpha$ -actinin (1:500, #3134; Cell Signaling Technology), anti-cardiac troponin T (cTnT) (1:250, 15513-1-AP; Proteintech, Wuhan, China), anti-Ki67 (1:250, 27309-1-AP; Proteintech), anti-SRY-Box Transcription Factor 2 (SOX2) (1:250, 11064-1-AP; Proteintech), anti-octamer-binding transcription factor 4 (OCT4) (1:200, #2750; Cell Signaling Technology), anti-stage-specific embryonic antigen 4 (SSEA4) (1:200, #4755; Cell Signaling Technology), and anti-TRA-1-60 (1:500, #4746; Cell Signaling Technology). Then, cells were washed and incubated with the following species-specific fluorescence-conjugated secondary antibodies: Alexa Fluor 488-labeled goat anti-rabbit or anti-mouse IgG, Alexa Fluor 594-labeled goat anti-rabbit or anti-mouse IgG (Thermo Fisher Scientific Inc.), according to the host species of the primary antibodies. The cells were then counterstained with 0.5  $\mu\text{g}/\text{mL}$  of 4',6'-diamidino-2-phenylindole (DAPI) (4083; Cell Signaling Technology) for 15 min at room temperature. After being washed

with phosphate-buffered saline (PBS), the chambers were mounted and observed under fluorescence microscopy (IX83; Olympus, Tokyo, Japan).

## 2.5. Flow cytometric analysis

The hiPSC-CMs were harvested by trypsinization and used to prepare a single-cell suspension in PBS ( $1 \times 10^6$  cells/mL). Then, the cells were fixed using 4% paraformaldehyde at room temperature for 20 min and washed twice with Flow Cytometry Perm Buffer (Proteintech). Then, the cells were incubated with primary antibodies against cTnT (1:100, MA5-12960; Invitrogen, Carlsbad, CA, USA) or  $\alpha$ -actinin (1:50, MA5-36095; Invitrogen) for 1 h at 4 °C. Mouse IgG1 served as the negative control. After centrifugation and two washes with  $1 \times$  PBS, the cells were incubated with anti-mouse IgG Alexa Fluor 488 or anti-mouse IgG Alexa Fluor 647 for 30 min at 4 °C. After centrifugation and two washes with  $1 \times$  PBS, cells were resuspended in 500  $\mu$ L of  $1 \times$  PBS and analyzed by flow cytometry (BD FACSymphony A3, Franklin Lakes, NJ, USA). Data analysis was performed using NovoExpress (v.1.5.4; Agilent, Santa Clara, CA, USA).

## 2.6. Reverse transcription real-time quantitative polymerase chain reaction (RT-qPCR)

TRIzol reagent (Thermo Fisher Scientific Inc.) was used to isolate total RNA from cell samples. A QuantiTect Reverse Transcription Kit (Qiagen, Hilden, Germany) was used to reversely transcribe complementary DNA from total RNA samples, following the manufacturer's instructions. The expression of genes was detected by qPCR using SYBR Green RT PCR Mix (Qiagen). The following settings were used: 95 °C for 2 min, 40 cycles of 95 °C for 20 s, and 60 °C for 15 s. Primers provided in Table 1 were used for amplification. The relative gene expression was calculated using the  $2^{-\Delta\Delta Ct}$  method and normalized to that of glyceraldehyde-3-phosphate dehydrogenase (GAPDH).

## 2.7. Western blotting and dot blotting

Radioimmunoprecipitation assay (RIPA) lysis buffer (Cell Signaling Technology) was used to lyse the cell and tissue samples. For subcellular fractions, NE-PER nuclear and cytoplasmic extraction reagents (#78833; Thermo Fisher Scientific Inc.) were used. Protein concentrations were determined using the Pierce BCA Protein Assay Kit (Thermo Fisher Scientific Inc.). For tissue-based Western blotting, lysates were prepared from peri-infarct regions. Then, 30  $\mu$ g of protein from each sample was loaded onto the gel and subjected to sodium dodecyl sulfate-polyacrylamide gel electrophoresis. The samples were then transferred onto nitrocellulose (NC) membranes, which were blocked overnight with 3% (V/V) bovine serum albumin (BSA), and 0.1% (V/V)  $\text{NaN}_3$  in PBS at 4 °C. The membranes were incubated with the following primary antibodies and dilutions at 4 °C overnight: anti-NKX2.5 (1:1000, #8792; Cell Signaling Technology), anti- $\alpha$ -SMA (1:1000, #19245; Cell Signaling Technology), anti-versican (1:2000, ab177480; Abcam, Cambridge, UK), anti-chondroitin sulfate (anti-CS, 1:1000, ab11570, Abcam), anti-CCL2 (1:1000, 25542-1-AP; Proteintech), anti-NODAL (1:1000, ab55676; Abcam), anti-GDF11 (1:1000, 26715-1-AP; Proteintech), anti-Wnt16 (1:1000, 28610-1-AP; Proteintech), anti-CCL8 (1:1000, ARG56709; Arigo, Shanghai, China), anti-p-Drosophila mothers against decapentaplegic protein (SMAD)2/3 (1:1000, #8828; Cell Signaling Technology), anti-SMAD2/3 (1:1000, #5678; Cell Signaling Technology), anti-mHapln1 (1:1000, ab181997; Abcam, Cambridge, UK), anti-lamin B1 (1:1000, 12987-1-AP; Proteintech), anti-TNNT13 (1:500, MA1-20112; Thermo Fisher Scientific Inc.), anti-MYL2 (1:1000, 10906-1-AP; Proteintech), anti-P21 (1:1000,

**Table 1**

The primers for real-time quantitative polymerase chain reaction (RT-qPCR).

Genes	Forward (5'-3')	Reverse (5'-3')
Human		
MYH7	GGAGTTCACACGCCTCAAGAG	TCCTCAGCATCTGCCAGGTGT
MYH6	GGAAGACAAGGTCAACAGCCTG	TCCAGTTCCCGCTTGTCTCGCT
MYL2	TGAGAGACACCTTTGTCTGCC	GGGTCCGCTCCCTAAGTTT
MYL7	AAGCCATCTGAGTGCCTTC	AACATCTGTCCACCTCAGC
TNNI3	CTAGTGGCTTGATCCAGCA	GCTTCAGGAGTGTGACAATGGC
TNNI1	CCAACCTCAAGTCTGTGAAGAAG	TCGGAGACTTGGCGGCATCAA
PLN	AGCACGTCAAAAGCTACAGAATCT	GCTGATGTGGCAAGCTGCAGATC
ATP2A2	GGACTTTGAAGCGGTGATTGTG	CTCAGCAAGGACTGGTTTTTCGG
RYR2	CTTGAGGTTGGCTTCTGCCAG	TGTGCCAGCAAAGAGAGGAGCA
KCNJ2	AACAGTGCAGGAGCCGCTTGT	AGGACAAAGCCAGGAGCAAGA
SCN5A	CAAGACCTGCTACCACATCGTG	GTCGGCATACTCAAGCAGAACC
CACNA1C	GCAGGAGTACAAGAACTGTGAC	CGAAGTAGTGGAGTTGACCAC
RUNX1	CCCACTATGAGAGTAGGTGTCC	GGGTAAGACTGGTTCATAGGACC
DAB2	CTCTGTCCAGTCTCACCACAT	GTCTCGAGACGGAGGAGCAAA
NKX2.5	AAGTGTGCGTCTGCTTTCCCG	TTGTCCGCTCTGTCTTCTCCA
ACTA2	CTATGCCTCTGACGCACT	CAGATCCAGACGCATGATGGCA
GAPDH	GTCTCCTCTGACTTCAACAGCG	ACCACCTGTTGCTGTAGCCAA
Mouse		
HAPLN1	TACTGCTGTGGTGGCATTGGAG	GGTCAAAGGAAGCAATCACTGCC
GAPDH	CATCACTGCCACCAGAAGACTG	ATGCCAGTGGCTTCCCGTTACG

10355-1-AP; Proteintech), anti-Cyclin D1 (1:5000, 26939-1-AP, Proteintech), anti-Cyclin D2 (1:1000, 10934-1-AP; Proteintech), and anti-GAPDH (1:5000, 10494-1-AP; Proteintech). After the membranes were thoroughly washed, they were incubated with horseradish peroxidase (HRP)-conjugated secondary antibodies corresponding to the host species of the primary antibodies for 1 h min at room temperature. Then, the protein band signals were developed using SuperSignal West Dura (Thermo Fisher Scientific Inc.), in the ChemiDoc MP Imaging System (Bio-Rad, Irvine, CA, USA). Relative protein levels were quantified based on grayscale quantification from three repeats, using ImageJ (v1.5.1).

For dot blotting, anti-versican, anti-CS, and different concentrations of chemokines were spotted onto NC membranes and air-dried for 5 h. Then, the membranes were blocked overnight with the same blocking buffer described above. Subsequently, the membrane was incubated with biotinylated versican (3  $\mu$ g/mL) for 1 h at room temperature. After being washed, the membranes were incubated with HRP-conjugated streptavidin (1:2000, SA00001-0; Proteintech) for 1 h at room temperature. Bound versican was detected using the enhanced chemiluminescence (ECL) reagent described above.

## 2.8. Enzyme-linked immunosorbent assay (ELISA)

A Human Versican ELISA kit (ab283883; Abcam) was used to measure the concentration of versican levels in the culture medium of hiPSC-CMs, following the manufacturer's instructions. For analysis of the binding of GDF11 and NODAL to versican, 4-mm-diameter 96-well EIA/RIA plates (Corning Inc., Corning, NY, USA) were coated with versican (20 mg/mL) overnight at 4 °C. The plates were washed five times with  $1 \times$  PBS containing 0.05% Tween-20 (PBST) and blocked with 10% fetal bovine serum in  $1 \times$  PBST for 2 h at room temperature. The versican-coated wells were incubated with serial dilutions of NODAL or GDF11 (0–3  $\mu$ g/mL) for 2 h. The wells were washed and then incubated with biotinylated anti-human GDF11 (1  $\mu$ g/mL, LS-C243834; LS-Bio, Seattle, WA, USA) or biotinylated anti-human NODAL (1  $\mu$ g/mL) in PBST and 1% fetal bovine serum for 1 h at room temperature. After being washed, the wells were incubated with HRP-conjugated streptavidin (1:2000, SA00001-0; Proteintech) for 1 h, and the optical density was read at 490 nm in a microtiter plate reader.

In the indicated experimental groups, immobilized versican was treated overnight at 37 °C with chondroitinase ABC (C'ABC) (0.6 units/

mL, pH 8.0), chondroitinase B (C'B) (0.06 units/mL, pH 8.0), or keratanase (KerA) (0.6 units/mL, pH 8.0). After blocking, NODAL or GDF11 (1 µg/mL) was added to the wells and incubated for 2 h at room temperature. Anti-versican and anti-CS (1 µg/mL) were used as controls for enzyme treatment, and HRP-conjugated anti-rabbit or anti-mouse IgG was used to detect the binding of the primary antibodies.

### 2.9. Myocardial infarction in adult mice

Myocardial infarction was induced in 12-week-old female C57BL/6J mice by ligating the left anterior descending (LAD) coronary artery. Mice were anesthetized with isoflurane and artificially ventilated with tracheal intubation. After a skin incision, lateral thoracotomy was performed in the third intercostal space through blunt anatomy of intercostal muscles. Following artery ligation, intramyocardial injections of rmHAPLN1 (50 µL at 2 µg per mouse) or PBS were administered. The chest wall incision was sutured with 6.0 non-absorbable silk thread, and the wound was sealed with skin adhesive. The mice were then heated for several minutes until recovery. To record cell proliferation *in vivo*, we administered an intraperitoneal injection of 5 mg/kg EdU 10 days after myocardial infarction. The hearts were collected 21 days later for EdU, Ki67, and AURKB visualization. Additionally, mice in the treatment and control groups were euthanized using carbon dioxide for heart collection 4, 14, and 35 days after myocardial infarction, following the American Veterinary Medical Association (AVMA) Guidelines for the Euthanasia of Animals (2020 Edition).

### 2.10. Echocardiography

Mice were isoflurane-sedated and then subjected to heart function evaluation by transthoracic echocardiography using a Vevo 3100 VisualSonics device (FujiFilm, Tokyo, Japan). All echocardiography measurements were performed by a sonologist without authorship in this study.

### 2.11. Histological and immunofluorescent examination

The hearts of mice were fixed in 4% paraformaldehyde, embedded in paraffin, and sectioned. For the analysis of juvenile and adult cardiac regeneration following myocardial infarction, serial sections were cut through the entire ventricle from apex to base at 0.4 mm intervals. Fibrosis was detected using Masson's trichrome staining. The section containing the papillary muscle region was used to quantify scar size using ImageJ software, based on Masson's trichrome staining. The relative scar size was calculated by comparing it to the total section size.

### 2.12. Statistical analysis

GraphPad Prism 8.1.0 (GraphPad Software, La Jolla, CA, USA) was utilized to conduct the statistical analysis. The data are presented as mean ± standard deviation (SD). One-way analysis of variance (ANOVA) with Turkey post hoc tests and two-way ANOVA with Bonferroni correction for post-hoc comparisons were used for analyses as indicated. Unpaired Welch's *t*-test was performed for two group comparisons. Significance was defined as  $P < 0.05$ .

## 3. Results

### 3.1. Characterization of hiPSC-CMs

To characterize the pluripotent properties of iPSCs, we compared the expression of multiple pluripotent and self-renewal marker genes between iPSCs and commercial hESCs. RT-qPCR

assays confirmed similar expression of the pluripotent marker genes (*OCT4*, *SOX2*, *NANOG* and *KLF4*) (Fig. S1A) and self-renewal marker genes (*MKI67* and *AURKB*) (Fig. S1B). Immunofluorescence (IF) staining confirmed the protein expression of a self-renewal marker (Ki-67) and pluripotent markers (*OCT4*, *SOX2*, *SSEA4*, and *TRA-1-60*) in iPSCs (Fig. S1C). Then, we induced iPSC-CMs using the GiWi protocol [14] (Fig. S2A). The expression of the cardiac progenitor cell (CPC) marker *NKX2.5* was assessed by RT-qPCR on the indicated days (Fig. S2B), which was confirmed by the IF staining (Fig. S2C). Moreover, the cardiomyocyte markers *ACTN1* (Figs. S2D and E) and *TNNT2* (Fig. S2F and G) were also elevated after the induction by results of RT-qPCR and IF. Flow cytometric analysis further confirmed that over 95% of the hiPSC-CMs had positive expressions of  $\alpha$ -actinin and cTnT (Figs. S2H and I).

### 3.2. Hapln1 promotes the proliferation of hiPSC-CMs in a dose-dependent manner

Since Hapln1 can promote the dedifferentiation and proliferation of cardiomyocytes during regeneration [13], we assessed whether recombinant rhHapln1 can modulate the proliferation of hiPSC-CMs. After treatment with varied concentrations (0, 20, 100, and 500 ng/mL) of rhHapln1 for 48 h, cells were subjected to IF staining for proliferation markers (EdU and Ki67). The results showed that rhHapln1 dose-dependently promoted the proliferation of hiPSC-CMs (Figs. 1A–D).

Then, we analyzed the influence of rhHapln1 on hiPSC-CM maturity by assessing the *MYH7/MYH6*, *MYL2/MYL7*, and *TNNI3/TNNI1* ratios [5]. After 4 weeks (4W) of culture in RPMI/B27 with insulin, the *MYH7/MYH6*, *MYL2/MYL7* and *TNNI3/TNNI1* ratios were significantly higher than those at 2W. However, when rhHapln1 (100 ng/mL) was added during the last two weeks of culture, the increase of the ratios was substantially weakened (Fig. 1E). After that, we assessed the expression of  $Ca^{2+}$  handling genes (*PLN*, *ATPA2*, and *RYR2*) and ion channel genes (*KCNJ2*, *SCN5A*, and *CACNA1C*), which are critical for cardiac muscle contraction and relaxation [16], circadian rhythms, and electrophysiology [17]. The results showed that hiPSC-CM maturation was associated with increased expression of these genes (Figs. 1F and G). However, these alterations were partially reversed (except *ATPA2* and *CACNA1C*) by rhHapln1 treatment (Figs. 1F and G).

Since we observed the inhibitory effect of rhHapln1 on hiPSC-CM maturation, we further explored whether it induced hiPSC-CM dedifferentiation based on the markers of dedifferentiation, including *RUNX1*, *DAB2*, *NKX2.5*, and *ACTA2*. rhHapln1 treatment significantly retained the expression of *RUNX1*, *NKX2.5*, and *ACTA2*, which were lost during maturation (Fig. 1H). The retention of *NKX2.5* and *ACTA2* resulted from the hHapln1 was confirmed by Western blotting at the protein level (Figs. 1I and J). Since the maturation of hiPSC-CMs is associated with increased susceptibility to hypoxia-induced damage [18], we tested their viability under hypoxic culture and hypoxia-induced cytotoxicity by CCK-8 and LDH release assays, respectively (Figs. 1K and L). After hypoxic treatment, 4W hiPSC-CMs had significantly lower viability and were more susceptible to re-oxygenation-induced injury (reflected by LDH release) than 2W hiPSC-CMs. However, these effects were alleviated in the rhHapln1-treated group (Figs. 1K and L). Terminal deoxynucleotidyl transferase dUTP nick end labeling (TUNEL) staining confirmed that hypoxia-induced apoptosis was weakened by rhHapln1 treatment (Figs. 1M–O).

### 3.3. Versican binds with NODAL and GDF11

Hapln1 can stabilize the interaction between HA and versican, two critical ECM components essential for cardiac development

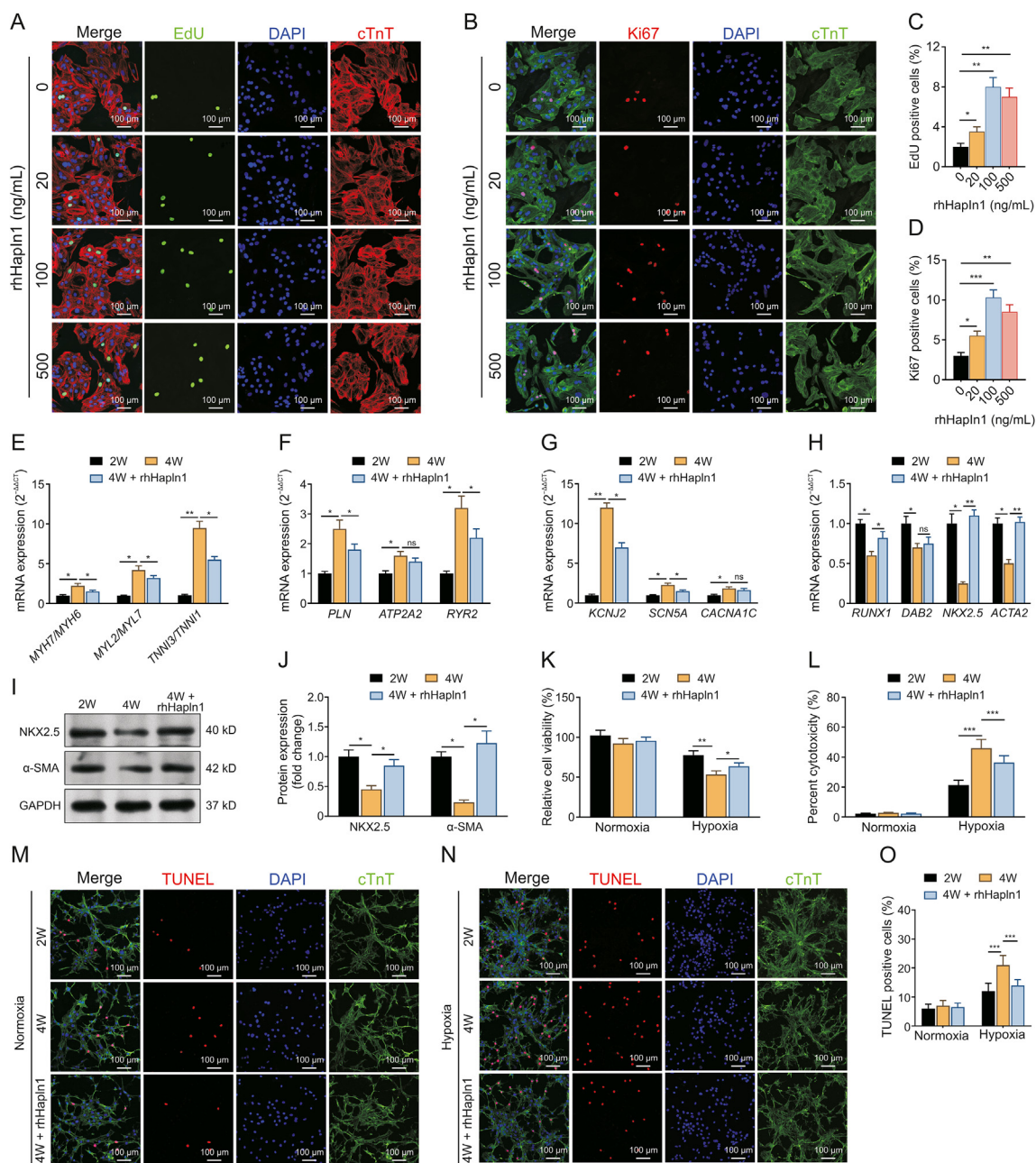


**Fig. 1.** Recombinant human hyaluronan and proteoglycan link protein 1 (rhHapl1) promotes the proliferation and dedifferentiation of human induced pluripotent stem cell-derived cardiomyocytes (hiPSC-CMs) in a dose-dependent manner. (A–D) After administration of various concentrations (0, 20, 100, and 500 ng/mL) of rhHapl1 for 72 h, proliferation markers of the hiPSC-derived cardiomyocytes were tested using immunofluorescence analysis. (A, C) Representative immunofluorescence (IF) images of the EdU incorporation assay and quantification of EdU-positive hiPSC-CMs ( $n = 3$ ). (B, D) Representative IF images of Ki67 staining and quantification of Ki67-positive hiPSC-CMs ( $n = 3$ ). (E–G) Real-time quantitative polymerase chain reaction (RT-qPCR) assays were used to test markers for cardiomyocyte maturity. (H) QPCR was used to assess dedifferentiation markers (*RUNX1*, *DAB2*, *NKX2.5*, and *ACTA2*) of hiPSC-CMs. (I, J) Immunoblots were performed to assess markers for hiPSC-CM dedifferentiation (*NKX2.5*,  $\alpha$ -SMA, encoded by *ACTA2* gene) as shown by the (I) representative blot images and (J) grayscale quantification. (K, L) 24 h after hypoxic treatment, cells were subjected to 6 h reoxygenation. Then, Cell Counting Kit (CKK)-8 and lactate dehydrogenase (LDH)-release assays were performed to detect (K) cell viability and (L) LDH cytotoxicity. (M–O) Terminal deoxynucleotidyl transferase dUTP nick end labeling (TUNEL) staining was conducted to detect cell apoptosis. One-way analysis of variance (ANOVA) with Turkey post hoc tests was conducted for multiple group comparisons in Figs. 1C and D, while two-way ANOVA with Bonferroni correction for post-hoc comparisons was used for the remaining comparisons. Data are presented as the mean  $\pm$  standard deviation ( $n = 3$ ). \* $P < 0.05$ , \*\* $P < 0.01$ , and \*\*\* $P < 0.001$ . DAPI: 6-diamidino-2-phenylindole; cTnT: cardiac troponin T; ns: not significant.

[10]. ELISA data confirmed that rhHapl1 increased versican levels in the culture medium from hiPSC-CMs in a dose-dependent manner (Fig. 2A). The concentration of versican in the culture medium from the 100 ng/mL hpHapl1-treated hiPSC-CMs was approximately 2-fold higher than that from the untreated hiPSC-CMs (Fig. 2A). Therefore, the effects of Hapl1 on the

dedifferentiation and proliferation of hiPSC-CMs might be mediated by versican. Versican can interact with a series of cytokines/chemokines that modulate cellular responses [19,20]. Thus, it is reasonable to assume that some of the cytokines/chemokines might participate in the dedifferentiation and proliferation processes. The proteins with known or potential interactions with

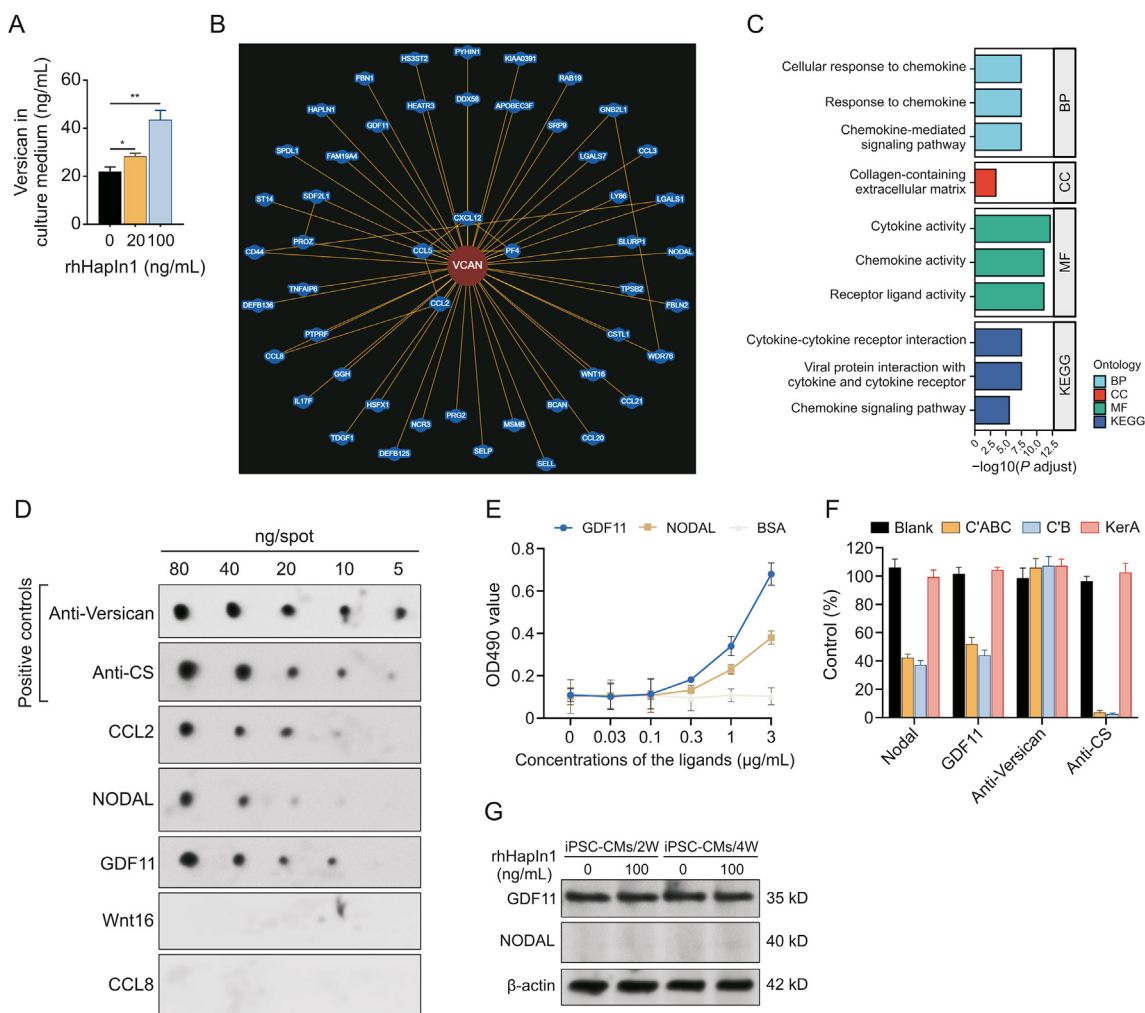


**Fig. 2.** Versican binds with Nodal growth differentiation factor (NODAL) and growth differentiation factor 11 (GDF11). (A) Enzyme-linked immunosorbent assays (ELISAs) were performed to detect the concentration of versican in the culture medium of human induced pluripotent stem cell-derived cardiomyocytes (hiPSC-CMs) after 72 h recombinant human hyaluronan and proteoglycan link protein 1 (rhHapln1) treatment. (B) Proteins with validated/potential interactions with versican. (C) Gene Ontology (GO)/Kyoto Encyclopedia of Genes and Genomes (KEGG) analysis of the genes encoding the proteins in panel B. (D) Binding of versican to selective chemokines. Anti-versican, anti-chondroitin sulfate (anti-CS) mAb CS56, or selective chemokines (5–100 ng/spot) were spotted onto nitrocellulose membranes. After blocking, biotinylated versican (3 μg/mL) was applied to the membrane. The binding of biotinylated versican was detected in immunoblotting. (E) Binding of NODAL or GDF11 to immobilized versican. Serial dilutions of NODAL or GDF11 (0–3 μg/mL) were added to the versican (300 ng/well)-coated wells and incubated for 2 h. After washing, the binding of chemokines to versican was measured by ELISAs. (F) Versican binds NODAL and GDF11 through glycosaminoglycan chains. Versican (300 ng/well) was coated onto the wells of an ELISA plate. After blocking, the wells were untreated or treated with chondroitinase ABC (C'ABC), chondroitinase B (C'B), or keratanase (KerA) overnight at 37 °C. After washing, binding of Nodal (1 μg/mL), anti-versican core protein mAb (3 μg/mL), or anti-CS mAb (1:500 dilution) was detected. Values are expressed as the percentage of specific binding compared with the control. (G) Western blotting assays were conducted to investigate the effect of Hapln1 on the expression of GDF11 in hiPSC-CMs (2 and 4 weeks (W)), with or without the treatment of rhHapln1 (100 ng/mL) for 72 h. One-way analysis of variance (ANOVA) with Turkey post hoc tests was conducted for multiple group comparisons ( $n = 3$ ). \* $P < 0.05$  and \*\* $P < 0.01$ .

versican were identified using BioGrid (<https://thebiogrid.org/>) (Fig. 2B). Then, the genes encoding these proteins were subjected to Gene Ontology (GO)/Kyoto Encyclopedia of Genes and Genomes (KEGG) analysis (Fig. 2C). The results showed that *CCL2/CCL20/CCL21/CCL3/CCL5/CCL8/CXCL12/FBN1/GDF11/IL17F/NODAL/PF4/SLURP1/TGDF1/WNT16* are included in the receptor ligand activity (Fig. 2C and Table S1). Among them, GDF11 and NODAL belong to TGF- $\beta$ s subfamily members. TGF- $\beta$ /SMAD signaling is implicated in cardiomyocyte proliferation during development and in the setting of cardiac regeneration [21]. NODAL and GDF11 can bind to cell membrane receptors to phosphorylate the intracellular downstream SMAD2/3 [22]. Inhibition of TGF- $\beta$ /SMAD3 signaling can disrupt cardiomyocyte cell cycle progression and proliferation [23]. Therefore, we typically focused on this signaling pathway.

Dot blot analysis was performed to examine the binding of versican to specific chemokines, including CCL2, NODAL, GDF11,

Wnt16, and CCL8. Nitrocellulose membranes were used to spot the chemokines, followed by the addition of biotinylated versican. After being washed, the binding proteins were detected. Positive controls for versican binding, including anti-versican (ab177480) and anti-chondroitin sulfate (CS, ab11570), were also spotted on the membrane. The results showed that biotinylated versican could bind to CCL2, NODAL, and GDF11. This molecule failed to bind Wnt16 and CCL8 (Fig. 2D). Then, a reverse binding assay was conducted, in which versican was coated on 96-well EIA/RIA plates. The binding of soluble NODAL and GDF11 to the immobilized versican was examined by ELISAs. The results indicated that versican bound NODAL and GDF11 in a dose-dependent manner (Fig. 2E).

To determine whether the chemokine binding is mediated by the chondroitin sulfate (CS) side chains or by the core protein domain, we examined the effect of chondroitin sulfate degrading enzymes on the binding. Versican (300 ng/well) was coated onto

the wells of an ELISA plate and treated with chondroitinase ABC (C'ABC) or chondroitinase B (C'B). Both C'ABC and C'B treatments impaired the binding of versican to NODAL and GDF11. These two enzymes did not influence the binding between versican and anti-versican. In addition, C'ABC and C'B treatment almost completely abolished the reactivity of versican with the anti-CS antibody. In comparison, keratanase (KerA, which served as a negative control) failed to alter the binding of versican to these proteins (Fig. 2F).

### 3.4. *rhHapln1* promotes hiPSC-CM proliferation via the TGF- $\beta$ /SMAD2/3 signaling

Western blotting assays confirmed that *GDF11* is expressed by hiPSC-CMs, and this expression was unaffected by *rhHapln1* treatment. However, nodal expression was quite limited in these cells (Fig. 2G). The expression of *GDF11* and *NODAL* at the single-cell level in normal human fetal heart tissues was assessed using

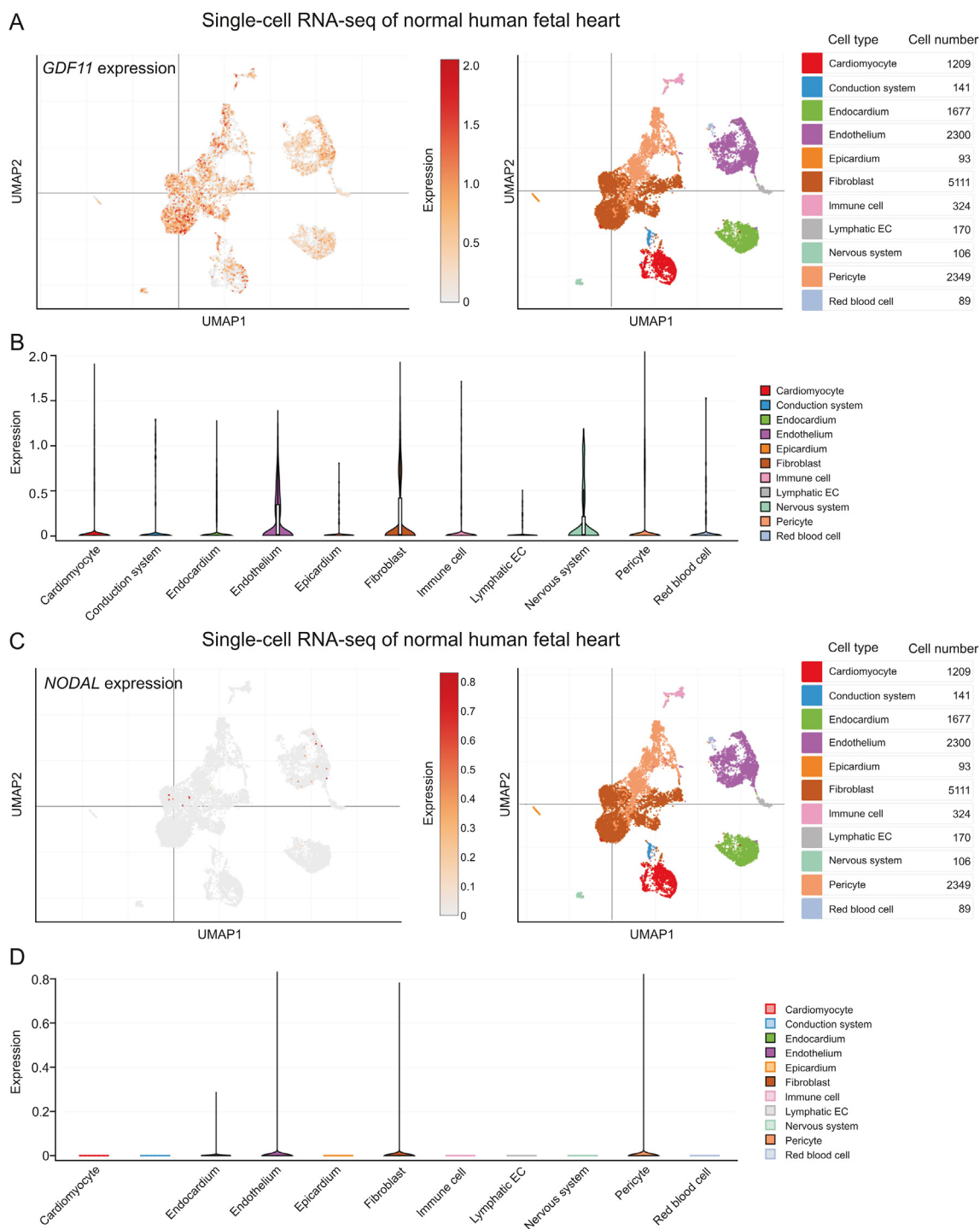


**Fig. 3.** *NODAL* and *GDF11* mRNA expression in fetal human hearts at the single-cell level. (A, C) Uniform manifold approximation and projection (UMAP) plot indicating the individual cells with *GDF11* (A) or *NODAL* (C) expression in the human fetal heart (left) and the cell type distribution (right). (B, D) Boxplots comparing different types of fetal cardiac cells with (B) *GDF11* or (D) *NODAL* expression. Images were generated with access provided by Single Cell Portal ([https://singlecell.broadinstitute.org/single\\_cell](https://singlecell.broadinstitute.org/single_cell)).

previous single-cell RNA sequencing (RNA-seq) datasets [24]. *GDF11* was extensively expressed by different types of cells, including cardiomyocytes and fibroblasts (Figs. 3A and B). In contrast, *NODAL* was not expressed in fetal heart cardiomyocytes (Figs. 3C and D). With another single-cell RNA-seq data from adult human heart tissues [25], *GDF11* expression was confirmed in adult cardiomyocytes (Figs. S3A and B). *NODAL* expression was also observed in adult cardiomyocytes, with lower expression and a smaller proportion of positive cells (Figs. S3C and D).

Therefore, the involvement of *GDF11* and the downstream TGF- $\beta$ -SMAD2/3 signaling pathway was further explored. *GDF11* uses canonical receptors and SMAD proteins for signaling [26]. Upon binding to activin receptors type II A or B, the *GDF11* dimer recruits and transphosphorylates activin-like kinase receptors, particularly ALK4, 5, or 7 [27]. In 4W hiPSC-CMs, we found that rhHapln1 treatment significantly enhanced SMAD2/3 phosphorylation in the nucleus (Fig. 4A). In addition, rhHapln1 induced downregulation of *TNNI3* and upregulation of *MYL2*,  $\alpha$ -SMA, and *NKX2.5*. These effects were significantly weakened by A-83-01 (a potent inhibitor of TGF- $\beta$  type I receptor ALK4, ALK5, and ALK7 kinase) (Fig. 4B). A-83-01 treatment also inhibited rhHapln1-induced cell proliferation (Figs. 4C–F). Furthermore, rhHapln1 treatment enhanced the expression of Cyclin D1 and D2 but reduced the expression of p21 (Fig. 4G). Similarly, these effects were hampered by A-83-01 treatment (Fig. 4G). These results suggest that rhHapln1-dependent cell cycle reentry was involved in the proliferation of cardiomyocytes.

### 3.5. Versican-based *GDF11* trapping is required for the proliferation-promoting effects of *Hapln1*

To explore whether the proliferation-promoting effects of *Hapln1* are *GDF11* dependent, we assessed whether the regulatory effects of rhHapln1 was influenced by the presence of exogenous *GDF11* or anti-*GDF11*. Western blotting assay was performed to test the downstream TGF- $\beta$ -SMAD2/3 signaling pathway. It was showed that *GDF11* could amplify the level of SMAD2/3 phosphorylation induced by the hHapln1 despite *GDF11* alone had no effect (Fig. 5A). And vice versa, hHapln1-induced upregulation of phosphorylated SMAD2/3 was mitigated with anti-*GDF11* (Fig. 5A). Consequently, expression of dedifferentiation markers (*NKX2.5* and  $\alpha$ -SMA) and maturation markers (*TNNI3* and *MYL2*) induced by *Hapln1* was additionally amplified with *GDF11* treatment as demonstrated with the results of Western blotting (Fig. 5B). on the contrary, anti-*DGF11* negatively regulated the effect of *Hapln1* (Fig. 5B). Moreover, Western blotting result showed that enhancement of proliferation-promoting effects of *Hapln1* by *GDF11* was partially dependent on the modulation of cell cycle related proteins indicated by the decreased cyclin-dependent kinase inhibitor P21 versus raised levels of Cyclin D1 and D2, activators of cell cyclin-dependent kinases) (Fig. 5C).

To further investigate whether the proliferation-promoting effects of *Hapln1* are versican dependent, we assessed the regulatory effects of *VCAN* knockdown on *HAPLN1* treatment alone or in combination with *GDF11*. It was showed by the Western blotting result that hHiPSC-CMs with *VCAN* knockdown had impaired responses to rhHapln1-induced SMAD2/3 phosphorylation (Fig. 5D), dedifferentiation (Fig. 5E), and cell cycle re-entrance (Fig. 5F). In addition, the additional effects of exogenous *GDF11* in the hiPSC-CMs was significantly mitigated with *VCAN* knockdown (Figs. 5D–F). These findings indicated that versican-based *GDF11* trapping is required for the proliferation-promoting effects of *HAPLN1*. It was further confirmed by results of IF staining regarding the proliferation markers (Figs. 5G–L).

### 3.6. *rmHapln1* induces cardiac regeneration in adult mice

For analysis of the therapeutic effects of *Hapln1* protein *in vivo*, adult mice were subjected to permanent ligation of the LAD artery and received a single intramyocardial injection of mouse *rmHapln1* (50  $\mu$ L at 2  $\mu$ g per mouse) or reconstitution buffer as a control.

The schematic diagram depicting LAD ligation and treatments in adult mice is provided in Fig. 6A. Masson's trichrome staining (Fig. 6B) and IF staining (Fig. 6C) of myocardial sections were performed to evaluate the indexes of fibrosis and cell-cycle re-entry. It was observed that significantly increased cardiomyocyte cell-cycle re-entry was induced by *rmHapln1* in the healthy myocardium adjacent to the infarcted region indicated by the increased percentage of Ki67, EdU and AURKB-positive cardiomyocytes (Fig. 6D). In comparison with the similar injured areas among groups at day 4, the scar areas were significantly reduced in the *rmHapln1*-treated group at day14 as shown by the result of Masson's trichrome (Fig. 6E). In addition, echocardiography results indicated that *rmHapln1* treatment improved cardiac function after myocardial infarction (Figs. 6F and G).

Western blotting assays were then performed using healthy myocardium adjacent to the infarcted region. In the control groups, phosphorylated SMAD2/3 in the nucleus and versican and *NKX2.5* expression were maintained at similar levels from day 4 to day 35 (Fig. 6H). In contrast, *rmHapln1* treatment increased the expression of phosphorylated SMAD2/3 in the nucleus and elevated the protein levels of versican and *NKX2.5* (Fig. 6I).

### 3.7. *rmHapln1* participates in fetal mouse heart proliferation and induces human iPSC-CM proliferation

*HAPLN1* has been characterized as a conserved gene in mammals. *HAPLN1* expression was abundant in endocardium and fibroblasts using previous single-RNA seq datasets from fetal human hearts [24] (Figs. S4A and B). However, its expression was drastically decreased in these cells in the adult human heart [25] (Figs. S4C and D). Similar trends were observed in the mouse heart [13]. Therefore, the loss of *Hapln1* during cardiac maturation might be one reason for the lost proliferative capability. To validate this hypothesis, we measured *HAPLN1* expression in the heart tissues of embryonic (E14) and postnatal mice (P1, P7, and P35). The results showed that *HAPLN1* expression was highly expressed in the embryonic heart but was substantially decreased in the postnatal heart (Figs. 7A–C). *rmHapln1* treatment also increased the ratio of EdU-positive and Ki-67 positive hiPSC-CMs (Figs. 7D–G). Since *Hapln1* is a secreted protein, primary cardiomyocytes or fibroblasts from P1 and P7 mice were collected to prepare conditioned culture mediums. Whether the conditioned medium from these cells could promote hiPSC-CM proliferation was tested. The conditioned medium from P7 cardiomyocytes or fibroblasts could not promote cell proliferation (Figs. 7H and I). However, the conditioned medium from P1 fibroblasts but not cardiomyocytes significantly enhanced hiPSC-CM proliferation. These effects were largely abrogated when the P1 primary fibroblasts had *HAPLN1* knockdown (Figs. 7H and I).

## 4. Discussion

Epicardial cells secrete factors during heart development and regeneration, including many ECM components [28,29]. ECM regulation by certain subgroups of epicardial cells might also play a critical role in localized cardiomyocyte proliferation during mammal heart development. As an important component of ECM, *Hapln1* has been characterized as an HA-organizing factor. A subset of epicardial fibroblasts expressing *HAPLN1A* envelops proliferative

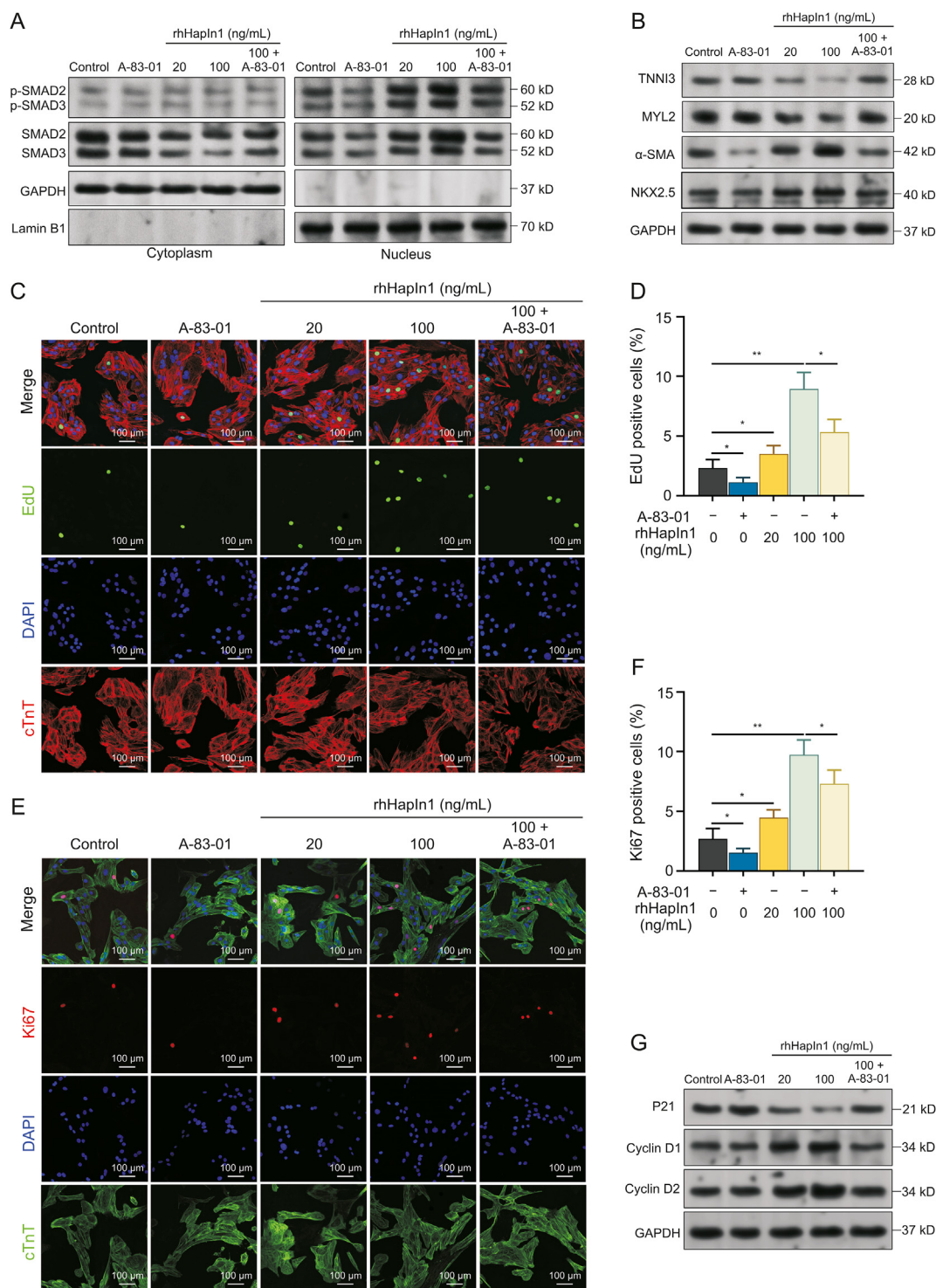


**Fig. 4.** Recombinant human hyaluronan and proteoglycan link protein 1 (rhHapln1) promotes human induced pluripotent stem cell-derived cardiomyocyte (hiPSC-CM) proliferation via the transforming growth factor (TGF)-β/SMAD2/3 signaling. (A) Western blotting assays were conducted in the cytoplasmic and nucleus fractions to explore the effect of HAPLN1 on the SMAD2/3 phosphorylation in hiPSC-CMs (4 weeks, (4W)). Cells were treated with 20 or 100 ng/mL rhHapln1 for 72 h, with or without the presence of A-83-01 (1 μM). (B) Western blotting assays were conducted to explore the expression of the hiPSC-CM maturation markers (TNNI3 and MYL2) and dedifferentiation markers (NKX2.5 and α-SMA) in whole-cell lysate from hiPSC-CMs as treated in panel A. (C–F) The proliferation of hiPSC-CMs as treated in Fig. 4A was investigated using (C, D) EdU incorporation assays and (E, F) immunostaining of Ki67. (G) Western blotting assays were conducted to explore the expression of P21, Cyclin D1, Cyclin D2 in whole-cell lysate from hiPSC-CMs treated as in Fig. 4A. Two-way analysis of variance (ANOVA) with Bonferroni correction for post-hoc comparisons (D and F) were conducted. Data are presented as the mean ± standard deviation (n = 3). \*P < 0.05 and \*\*P < 0.01. GAPDH: glyceraldehyde-3-phosphate dehydrogenase; DAPI: 6-diamidino-2- phenylindole; cTnT: cardiac troponin T.

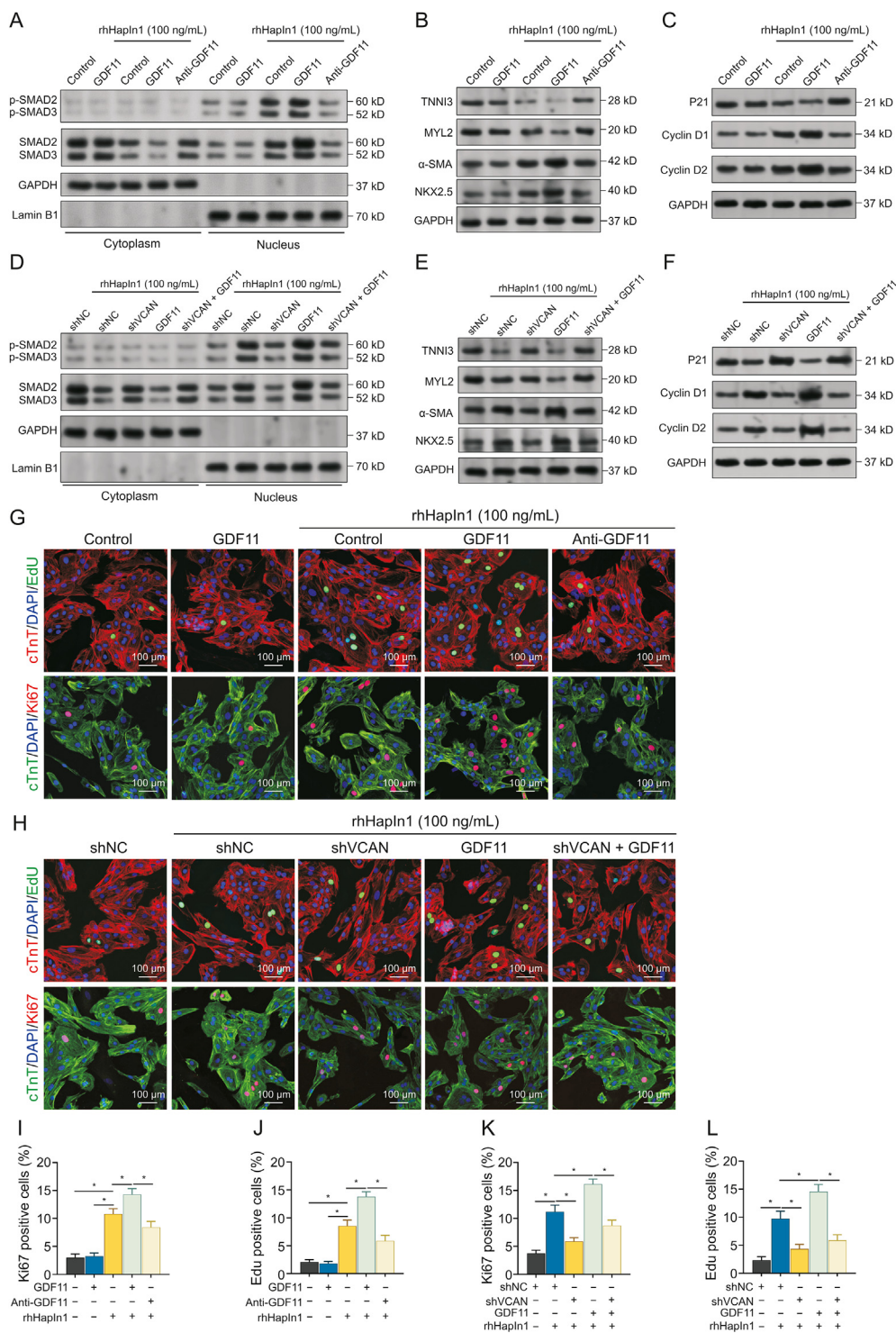


**Fig. 5.** Versican-based growth differentiation factor 11 (GDF11) trapping is required for the proliferation-promoting effects of hyaluronan and proteoglycan link protein 1 (Hapln1). (A) Western blotting assays were conducted in the cytoplasmic and nucleus fractions to explore the effect of GDF11 on HAPLN1-induced SMAD2/3 phosphorylation in hiPSC-CMs (4 weeks, (4W)). Cells were treated with 100 ng/mL Hapln1 for 48 h, with or without GDF11 (20 ng/mL) or GDF11-neutralizing antibody (anti-GDF11, 100 ng/mL). (B, C) Western blotting assays were conducted to explore the expression of (B) the human induced pluripotent stem cell-derived cardiomyocyte (hiPSC-CM) maturation markers (TNNI3 and MYL2), dedifferentiation markers (NKX2.5 and  $\alpha$ -SMA) and (C) cell-cycle related proteins (P21, Cyclin D1, and Cyclin D2) in whole-cell lysate from hiPSC-CMs, as treated in Fig. 5A. (D) Western blotting assays were conducted of the cytoplasmic and nucleus fractions, to explore the effect of VCAN manipulation on HAPLN1-induced SMAD2/3 phosphorylation in hiPSC-CMs (4W). Cells with or without lentivirus-mediated VCAN knockdown were treated with 100 ng/mL HAPLN1 for 72 h. One VCAN knockdown group received both HAPLN1 (100 ng/mL) and GDF11 (20 ng/mL) treatment. (E, F) Western blotting assays were conducted to explore the expression of (E) the hiPSC-CM maturation markers (TNNI3 and MYL2), dedifferentiation markers (NKX2.5 and  $\alpha$ -SMA) and (F) cell-cycle related proteins (P21, Cyclin D1, and Cyclin D2) in whole-cell lysate from hiPSC-CMs, as treated in Fig. 5D. (G–L) The proliferative abilities of hiPSC-CMs as treated in Figs. 5A and D, were investigated using EdU incorporation assays (G, I–J) and immunofluorescence staining of Ki67 (H, K–L). Two-way analysis of variance (ANOVA) with Bonferroni correction for post-hoc comparisons (G–J) was conducted. Data are presented as the mean  $\pm$  standard deviation ( $n = 3$ ).  $^*P < 0.05$ . GAPDH: glyceraldehyde-3-phosphate dehydrogenase; rhHapln1: recombinant human hyaluronan and proteoglycan link protein 1.

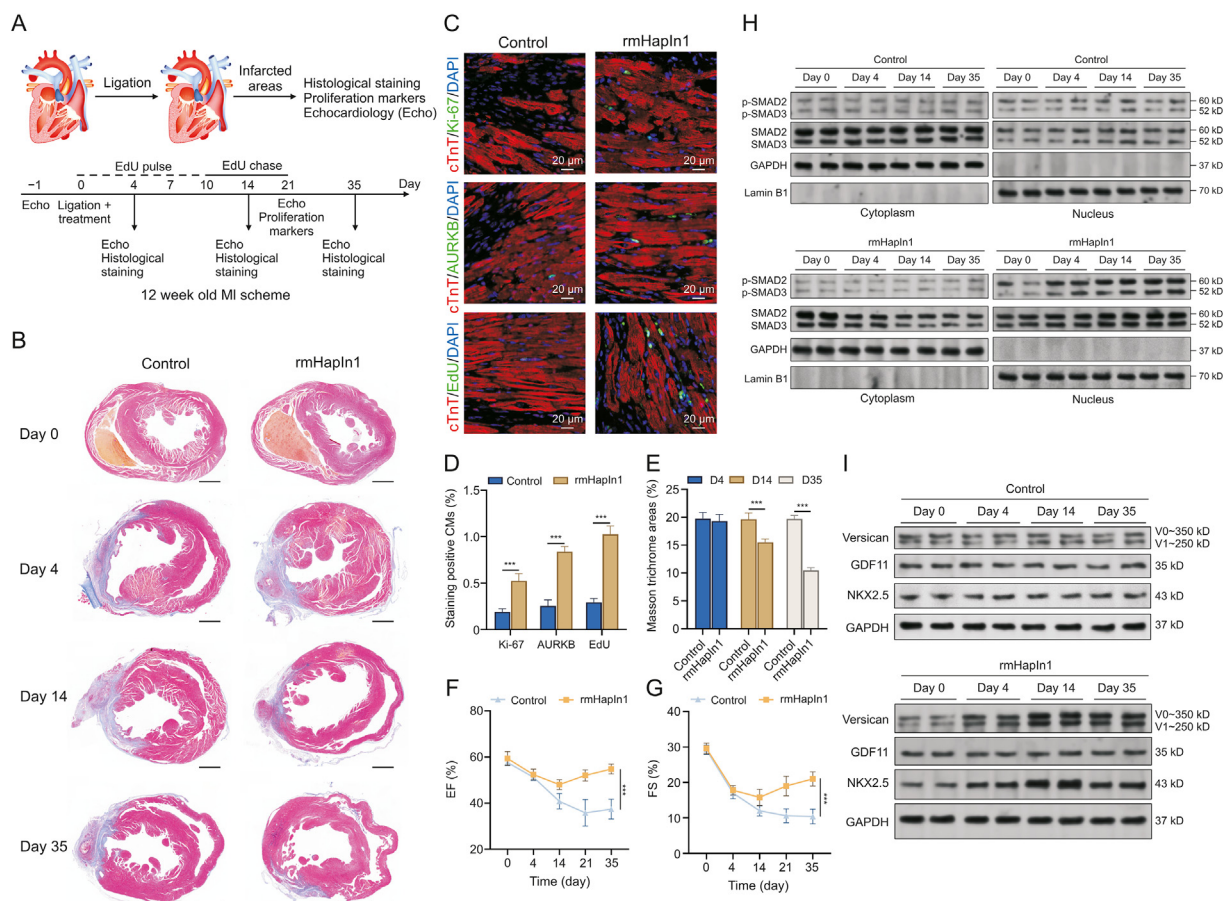


**Fig. 6.** Recombinant mouse hyaluronan and proteoglycan link protein 1 (rmHapln1) induced cardiac regeneration in adult mice. (A) A schematic diagram depicting left anterior descending (LAD) ligation in adult mice. (B, E) Heart section scar assessment following reconstitution buffer (control) or rmHapln1 treatment at indicated days after myocardial infarction (MI). Representative images are shown in Fig. 6B and were quantified in Fig. 6E ( $n = 6$  mice per group for days 0, 4, 15, and 35). (C) Representative images and (D) quantitation of *in vivo* evaluation of cardiomyocyte cell-cycle re-entry in the peri-infarct region 21 days after myocardial infarction by Ki67 (top), AURKB (middle), and EdU (bottom). Quantitation was conducted based on five random fields of peri-infarct areas from 6 PBS and 6 rmHapln1 samples. (F, G) Serial echocardiographic measurements of the ejection fraction (EF%) and fractional shortening (FS) ( $n = 6$  per group). Western blotting assays were conducted to assess (H) the phosphorylation of SMAD2/3 (H), versican, growth differentiation factor 11 (GDF11), and (I) NKX2.5 expression in the peri-infarct region at the indicated time points from tissues of two randomly selected mice in each group. Unpaired Welch's t-test was conducted in Figs. 6D–G. Data are presented as the mean  $\pm$  standard deviation ( $n = 3$ ). \*\*\* $P < 0.001$ .

cardiomyocytes during heart morphogenesis and regeneration [13]. In addition to HA, hapln1 also enhances the stability of versican in heart development [10]. During the differentiation of cardiomyocytes from hESCs, the major transcripts of versican all significantly increased in cardiomyocytes compared to hESCs, suggesting a potential role of versican in this process [30]. However, unlike the zebrafish hearts, the expression of hapln1 drastically decreased in adult human fibroblasts.

In this study, we tested the effect of exogenous rhHapln1 and found it promoted dedifferentiation and proliferation of hiPSC-CMs. In addition, the positive effect of Hapln1 on versican stability was verified in the culture medium of hiPSC-CMs. Versican comprises core proteins covalently linked to long chondroitin sulfate side chains. The chondroitin sulfate side chains bear many negative charges, enabling them to bind to a series of positively charged molecules such as certain growth factors, cytokines, and chemokines [31]. We searched the predicted potential Hapln1 binding proteins and focused on the chemokines involved in the receptor-ligand activity in KEGG analysis. Among the predicted chemokines, GDF11, a TGF- $\beta$ s subfamily member consistently expressed in fetal and adult human cardiomyocytes, could be trapped by versican via the chondroitin sulfate side chains.

The TGF- $\beta$ /SMAD signaling pathway is activated after ventricle ablation and is important in ventricle regeneration [23]. Inhibition of TGF type I receptors with the specific chemical inhibitor SB431542 completely abolished heart regeneration in zebrafish [32]. By stimulating the phosphorylation of SMAD2/3, GDF11 might enhance cardiomyocyte cell cycle progression and proliferation [21,23] and prevent cardiomyocyte hypertrophy [33]. In addition, GDF11 inhibits cardiomyocyte pyroptosis in mice with acute myocardial infarction via TGF- $\beta$ /SMAD2/3-mediated increases in HOXA3 [34] and mitochondrial biogenesis and telomerase activity [35]. Therefore, we hypothesized that GDF11 is an important downstream regulator of Hapln1. When GDF11 was neutralized or its downstream signaling was chemically inhibited in the culture system, rhHapln1-mediated hiPSC-CM dedifferentiation and proliferation were abolished. Similarly, when versican was knocked down, GDF11-mediated hiPSC-CM dedifferentiation and proliferation were abolished. In adult mice with induced myocardial infarction, mHapln1 significantly alleviated fibrosis and promoted cardiomyocyte proliferation. The trends of SMAD2/3 phosphorylation and NKX2.5 expression in the peri-infarct region were similar to the *in vitro* findings. Collectively, these findings indicated that Hapln1-mediated dedifferentiation and

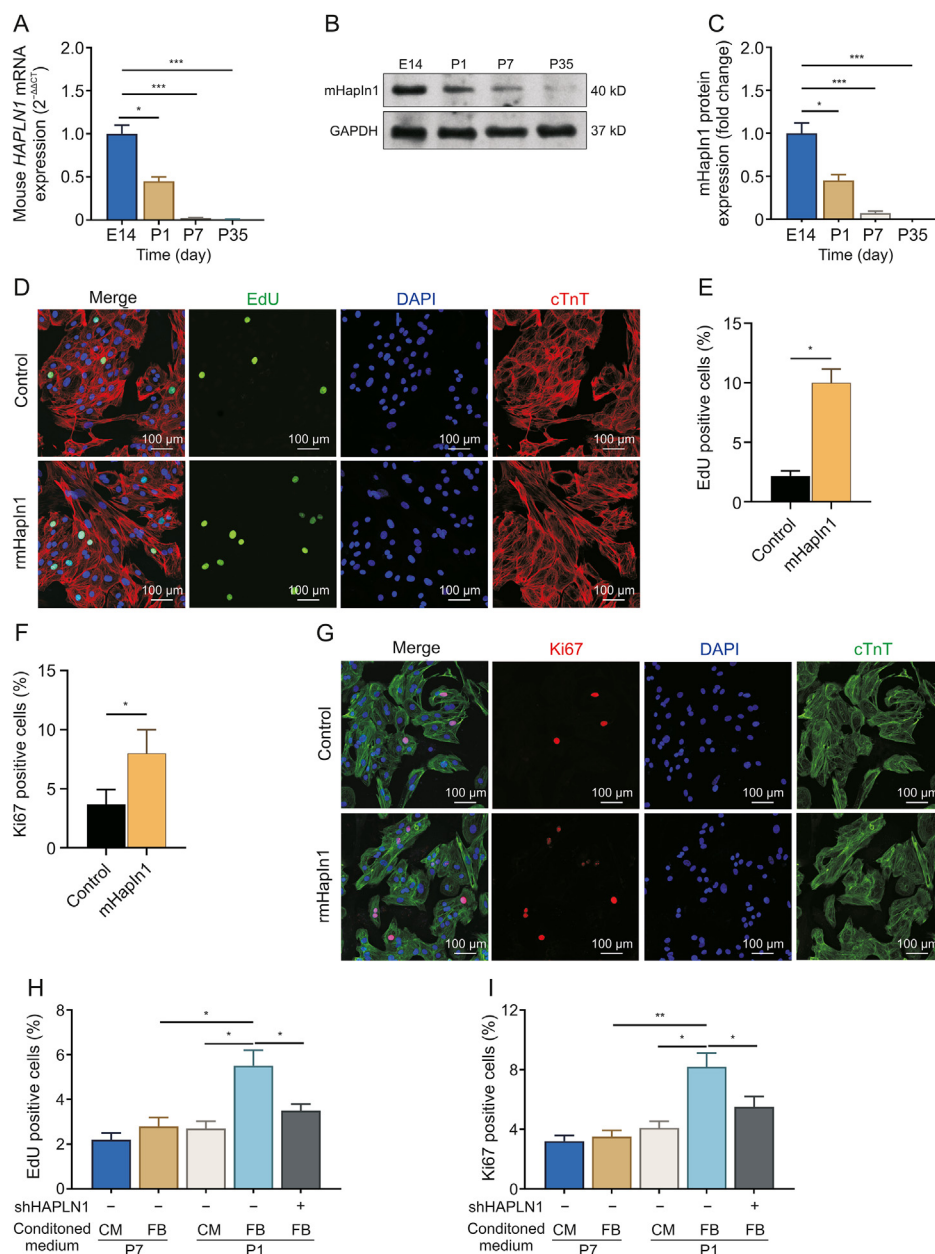


**Fig. 7.** Recombinant mouse hyaluronan and proteoglycan link protein 1 (rmHapln1) also induces human induced pluripotent stem cell-derived cardiomyocyte (hiPSC-CM) proliferation. (A) Real-time quantitative polymerase chain reaction (RT-qPCR) and (B, C) western blotting were conducted to evaluate the expression of *HAPLN1* at the mRNA and proteins levels in the heart tissues from embryonic (E14) and postnatal mice (P1, P7, and P35) (for qPCR,  $n = 5$ ; for Western blotting,  $n = 3$ ). The proliferative abilities of hiPSC-CMs (4weeks, (4W)) treated by rmHapln1 (100 ng/mL, 72 h) were investigated using (D, E) EdU incorporation assays and (F, G) immunostaining of Ki67. HiPSC-CMs (4W) were treated by conditioned medium from primary cardiomyocytes (CM) or fibroblasts (FB), with or without lentivirus-mediated *HAPLN1* knockdown from P1 or P7 mice heart tissues for 72 h. Then, cell proliferation was investigated using (H) EdU incorporation assays and (I) immunostaining of Ki67. One-way analysis of variance (ANOVA) with Turkey post hoc tests was conducted in Figs. 7A and C. Two-way ANOVA with Bonferroni correction for post-hoc comparisons was conducted in Figs. 7H and I. Unpaired Welch's t-test was conducted in Figs. 7E and F. Data are presented as the mean  $\pm$  standard deviation ( $n = 3$ ). \* $P < 0.05$  and \*\* $P < 0.01$ .

proliferation of hiPSC-CMs require versican-based GDF11 trapping. However, since the interaction between chondroitin sulfate side chains and GDF11 relies on the attraction between positive and negative charges, we could not exclude the possibility that some other chemokines are involved in hiPSC-CM dedifferentiation and proliferation.

Considering the multiple risks and technical hurdles of manipulating hiPSC-CM for regenerative therapy, Hapln1 might be an effective agent for hiPSC-CM dedifferentiation and proliferation. In addition, since Hapln1 exerts specific therapeutic values in

the mouse model of myocardial infarction, it is meaningful to explore its potential as a reagent for repairing damaged hearts in the future.

### 5. Conclusion

Hapln1 promotes dedifferentiation and proliferation of iPSC-derived cardiomyocytes by promoting versican-based GDF11 trapping and subsequent activation of the TGF- $\beta$ /SMAD2/3 signaling pathway. This molecule shows certain therapeutic values

in the mouse model of myocardial infarction. Therefore, Hapln1 might be an effective agent for hiPSC-CM dedifferentiation and proliferation and a potential reagent for repairing damaged hearts.

### CRediT author statement

**Ding-Jun Hao:** Investigation, Validation, Formal analysis, Writing - Original draft preparation; **Yue Qin:** Methodology, Writing - Original draft preparation, Reviewing and Editing; **Shi-Jie Zhou:** Conceptualization, Methodology; Formal analysis; **Bu-Huai Dong:** Methodology; **Jun-Song Yang:** Writing - Reviewing and Editing; **Peng Zou:** Supervision, Writing - Reviewing and Editing; **Li-Ping Wang:** Methodology; **Yuan-Ting Zhao:** Conceptualization, Investigation, Project administration, Supervision, Writing - Reviewing and Editing, Funding acquisition.

### Declaration of competing interest

The authors declare that there are no conflicts of interest.

### Acknowledgments

This study was supported by Shaanxi Province Natural Science Foundation, China (Grant No.: 2021JM-568).

### Appendix A. Supplementary data

Supplementary data to this article can be found online at <https://doi.org/10.1016/j.jpha.2023.09.013>.

### References

- [1] Y. Zhu, V.D. Do, A.M. Richards, et al., What we know about cardiomyocyte dedifferentiation, *J. Mol. Cell. Cardiol.* 152 (2021) 80–91.
- [2] W. Zhu, J. Sun, S.P. Bishop, et al., Turning back the clock: A concise viewpoint of cardiomyocyte cell cycle activation for myocardial regeneration and repair, *J. Mol. Cell. Cardiol.* 170 (2022) 15–21.
- [3] A.S.T. Smith, J. Macadangdang, W. Leung, et al., Human iPSC-derived cardiomyocytes and tissue engineering strategies for disease modeling and drug screening, *Biotechnol. Adv.* 35 (2017) 77–94.
- [4] M. Kleinsorge, L. Cyganek, Subtype-directed differentiation of human iPSCs into atrial and ventricular cardiomyocytes, *STAR Protoc* 1 (2020), 100026.
- [5] Y. Guo, W.T. Pu, Cardiomyocyte maturation: New phase in development, *Circ. Res.* 126 (2020) 1086–1106.
- [6] M. Zhao, S. Ye, J. Su, et al., Cardiomyocyte proliferation and maturation: Two sides of the same coin for heart regeneration, *Front. Cell Dev. Biol.* 8 (2020), 594226.
- [7] E. Bassat, Y.E. Mutlak, A. Genzelinakh, et al., The extracellular matrix protein agrin promotes heart regeneration in mice, *Nature* 547 (2017) 179–184.
- [8] D.A. Swann, S. Powell, J. Broadhurst, et al., The formation of a stable complex between dissociated proteoglycan and hyaluronic acid in the absence of a link protein, *Biochem. J.* 157 (1976) 503–506.
- [9] J. Govindan, M.K. Iovine, Hapln1a is required for connexin43-dependent growth and patterning in the regenerating fin skeleton, *PLoS One* 9 (2014), e88574.
- [10] E.E. Warrig, B.S. Snarr, M.R. Chintalapudi, et al., Cartilage link protein 1 (Crtl1), an extracellular matrix component playing an important role in heart development, *Dev. Biol.* 310 (2007) 291–303.
- [11] C.J. Derrick, J. Sánchez-Posada, F. Hussein, et al., Asymmetric Hapln1a drives regionalized cardiac ECM expansion and promotes heart morphogenesis in zebrafish development, *Cardiovasc. Res.* 118 (2022) 226–240.
- [12] J.M. González-Rosa, V. Martín, M. Peralta, et al., Extensive scar formation and regression during heart regeneration after cryoinjury in zebrafish, *Development* 138 (2011) 1663–1674.
- [13] J. Sun, E.A. Peterson, A.Z. Wang, et al., hapln1 defines an epicardial cell subpopulation required for cardiomyocyte expansion during heart morphogenesis and regeneration, *Circulation* 146 (2022) 48–63.
- [14] X. Lian, J. Zhang, S.M. Azarin, et al., Directed cardiomyocyte differentiation from human pluripotent stem cells by modulating Wnt/ $\beta$ -catenin signaling under fully defined conditions, *Nat. Protoc.* 8 (2013) 162–175.
- [15] F. Liu, Y. Fang, X. Hou, et al., Enrichment differentiation of human induced pluripotent stem cells into sinoatrial node-like cells by combined modulation of BMP, FGF, and RA signaling pathways, *Stem Cell Res. Ther.* 11 (2020), 284.
- [16] P. Ernst, P.A. Bidwell, M. Dora, et al., Cardiac calcium regulation in human induced pluripotent stem cell cardiomyocytes: implications for disease modeling and maturation, *Front. Cell Dev. Biol.* 10 (2023), 986107.
- [17] E.A. Schroder, M. Ono, S.R. Johnson, et al., The role of the cardiomyocyte circadian clocks in ion channel regulation and cardiac electrophysiology, *J. Physiol.* 600 (2022) 2037–2048.
- [18] M.C. Peters, R.G.C. Maas, I. van Adrichem, et al., Metabolic maturation increases susceptibility to hypoxia-induced damage in human iPSC-derived cardiomyocytes, *Stem Cells Transl. Med.* 11 (2022) 1040–1051 [LinkOut].
- [19] J. Hirose, H. Kawashima, O. Yoshie, et al., Versican interacts with chemokines and modulates cellular responses, *J. Biol. Chem.* 276 (2001) 5228–5234.
- [20] H. Kawashima, M. Hirose, J. Hirose, et al., Binding of a large chondroitin sulfate/dermatan sulfate proteoglycan, versican, to L-selectin, P-selectin, and CD44, *J. Biol. Chem.* 275 (2000) 35448–35456.
- [21] N.G. Frangogiannis, Transforming growth factor- $\beta$  in myocardial disease, *Nat. Rev. Cardiol.* 19 (2022) 435–455.
- [22] S. Li, J. Wu, TGF- $\beta$ /SMAD signaling regulation of mesenchymal stem cells in adipocyte commitment, *Stem Cell Res. Ther.* 11 (2020) 1–10.
- [23] Y. Peng, W. Wang, Y. Fang, et al., Inhibition of TGF- $\beta$ /Smad3 signaling disrupts cardiomyocyte cell cycle progression and epithelial–mesenchymal transition-like response during ventricle regeneration, *Front. Cell Dev. Biol.* 9 (2021), 632372.
- [24] M. Gu, Y. Miao, X. Zhou, et al., Abstract 238: single-cell transcriptomic analysis and patient-specific iPSCs reveal dysregulated cell cycle in coronary endothelial cell in hypoplastic left heart syndrome, *Circ. Res.* 127 (2020), A238.
- [25] N.R. Tucker, M. Chaffin, S.J. Fleming, et al., Transcriptional and cellular diversity of the human heart, *Circulation* 142 (2020) 466–482.
- [26] A. Simoni-Nieves, M. Gerardo-Ramírez, G. Pedraza-Vázquez, et al., GDF11 implications in cancer biology and metabolism. facts and controversies, *Front. Oncol.* 9 (2019), 1039.
- [27] A. Jamaiyar, W. Wan, D.M. Janota, et al., The versatility and paradox of GDF 11, *Pharmacol. Ther.* 175 (2017) 28–34.
- [28] X. Wang, Y. Lu, Y. Xie, et al., Emerging roles of proteoglycans in cardiac remodeling, *Int. J. Cardiol.* 278 (2019) 192–198.
- [29] L.A. Samsa, B. Yang, J. Liu, Embryonic cardiac chamber maturation: trabeculation, conduction, and cardiomyocyte proliferation, *Am. J. Med. Genet. C Semin. Med. Genet.* 163C (2013) 157–168.
- [30] C.K. Chan, M.W. Rolle, S. Potter-Perigo, et al., Differentiation of cardiomyocytes from human embryonic stem cells is accompanied by changes in the extracellular matrix production of versican and hyaluronan, *J. Cell. Biochem.* 111 (2010) 585–596.
- [31] Y. Wu, D.P.L. Pierre, J. Wu, et al., The interaction of versican with its binding partners, *Cell Res.* 15 (2005) 483–494.
- [32] F. Chablais, A. Jaźwińska, The regenerative capacity of the zebrafish heart is dependent on TGF $\beta$  signaling, *Development* 139 (2012) 1921–1930.
- [33] H. Zhu, L. Zhang, M. Zhai, et al., GDF11 alleviates pathological myocardial remodeling in diabetic cardiomyopathy through SIRT1-dependent regulation of oxidative stress and apoptosis, *Front. Cell Dev. Biol.* 9 (2021), 686848.
- [34] Z. Li, H. Xu, X. Liu, et al., GDF11 inhibits cardiomyocyte pyroptosis and exerts cardioprotection in acute myocardial infarction mice by upregulation of transcription factor HOXA3, *Cell Death Dis.* 11 (2020), 917.
- [35] L. Chen, G. Luo, Y. Liu, et al., Growth differentiation factor 11 attenuates cardiac ischemia reperfusion injury via enhancing mitochondrial biogenesis and telomerase activity, *Cell Death Dis.* 12 (2021), 665.